

Modelling of In-Nozzle Cavitation and Early Spray Breakup Using a Multiphase Volume of Fluid Method

H. Yu, L. Goldsworthy, P. Brandner and V. Garaniya

National Centre for Maritime Engineering and Hydrodynamics
Australian Maritime College, University of Tasmania, Launceston, Tasmania 7250, Australia.

Abstract

A compressible, multiphase Volume of Fluid Large Eddy Simulation is implemented in the OpenFOAM environment. The volume fraction transport equations for liquid, vapour and gas phases are reformulated to include phase change source terms. These terms are modelled with the cavitation model by Schnerr, which is extended to eliminate non-physical mass transfer rates. The numerical method is validated by comparing the simulated mass flow rates, pressure and liquid volume fraction distributions at different cavitation conditions against published experimental data. Favourable comparison between simulations and experiments is achieved with minor discrepancies attributable to uncertainties in fuel properties and assumptions made in numerical models. The application of the code to simulation of in-nozzle phenomena and primary breakup of the spray injected from a sharp edged nozzle reveals that in-nozzle flow separation, wall shear and cavitation contribute largely to the fragmentation of the jet.

Introduction

Modern diesel engines comprise multiple systems that govern complex combustion processes. The quality of combustion in the engine chamber has direct effects on the overall efficiency and emission of diesel engines. One of the main factors contributing to an efficient combustion cycle is the degree to which the diesel spray is atomised. The atomisation of a diesel spray can be attributed to interaction with ambient gas and in-nozzle flow characteristics such as flow separation and cavitation. In this study, characteristics of in-nozzle flow particularly the onset of flow separation and cavitation which are often considered to be the main reason for primary breakup [11] are numerically investigated.

The onset of cavitation in diesel injectors has been reported to enhance atomisation of emerging diesel spray and increase the dispersion angle in many experimental studies [1, 3]. For a nozzle with a sharp inlet, the high pressure gradient and fluid inertia cause the flow to separate and form a region of contracted flow. This creates a recirculation zone in which pressure can reduce to or below vapour pressure. Cavities generated after the sharp entrance can build along the nozzle wall and may extend to the nozzle exit. Depending on the relative length of the cavities and nozzle, vapour bubbles may collapse outside of nozzle exit enhancing the jet breakup. However, there are situations where flow separation and cavitation can result in complete detachment of fluid flow from the nozzle wall. In those cases, air can be drawn into low pressure regions of the nozzle, resulting in hydraulic flip. Upon the occurrence of hydraulic flip, in-nozzle flow does not experience wall shear. Consequently, the effect of wall shear minimises and spray atomisation may be suppressed, which leads to a narrower spray [12].

Recently, implementation of the Volume of Fluid method for prediction of primary spray breakup with the effects of in-nozzle

flow has been reported by Ghiji *et al.* [4]. As compared to homogenous [10], Eulerian-Lagrangian Coupling [5] and two fluid models [6], the VOF method is advantageous because it is able to capture a sharp liquid-gas interface in a volume conservative manner. The incompressible two-phase VOF method has also been integrated with cavitation models to study internal nozzle cavitation and its effects on the emerging spray by Marcer *et al.* [7]. However, in diesel engines, liquid fuel, fuel vapour and air can often co-exist in the chamber and phase change due to either cavitation or evaporation occurs exclusively between fuel and its vapour. In addition, the injection of fuel may exceed the speed of sound in the gas phase within the chamber due to high injection pressure. Modelling the spray atomisation under diesel engine operating conditions therefore falls into the framework of compressible multiphase flow with phase change. Thus, the main objective of the present study is to develop a compressible multiphase VOF method with cavitation modelling capability for improved diesel spray simulations.

Description of the VOF Approach

The VOF method adds phase transport equations accounting for volume fractions of each phase to the governing equations. For a multiphase flow with phase change, transport equations for all phases can be written as

$$\frac{\partial(\rho_i \alpha_i)}{\partial t} + \nabla \cdot (\rho_i \alpha_i \mathbf{U}_i) = \dot{m} \quad (1)$$

$$\frac{\partial(\rho_v \alpha_v)}{\partial t} + \nabla \cdot (\rho_v \alpha_v \mathbf{U}_v) = -\dot{m} \quad (2)$$

$$\frac{\partial(\rho_i \alpha_i)}{\partial t} + \nabla \cdot (\rho_i \alpha_i \mathbf{U}_i) = 0 \quad (3)$$

where \dot{m} is the phase change mass transfer rate, subscripts l and v are for the liquid and vapour phases respectively, while i represents phases that do not take part in the phase change process. The rate of mass exchange can be expressed as

$$\dot{m} = \dot{m}^+ - \dot{m}^- \quad (4)$$

The rate of condensation \dot{m}^+ and vaporisation \dot{m}^- of the liquid phase on the phase interface is modelled by Schnerr and Sauer model [8]. Detailed implementation of this model is discussed in the next section.

$$\begin{cases} \nabla \cdot (\alpha \mathbf{U}_l) + \nabla \cdot (\alpha \mathbf{U}_v) + \nabla \cdot (\alpha \mathbf{U}_i) = \nabla \cdot \mathbf{U} \quad (a) \\ \nabla \cdot \mathbf{U} = - \left(\frac{\alpha_l}{\rho_l} \left[\frac{D \rho_l}{Dt} \right] + \frac{\alpha_v}{\rho_v} \left[\frac{D \rho_v}{Dt} \right] + \frac{\alpha_i}{\rho_i} \left[\frac{D \rho_i}{Dt} \right] \right) + \dot{m} \left(\frac{1}{\rho_l} - \frac{1}{\rho_v} \right) \quad (b) \end{cases} \quad (5)$$

By adding and subtracting $\nabla \cdot (\alpha \mathbf{U})$ on the LHS of equation (1-3), expanding the convection terms and utilising equation (5), the final form of the multiphase transport equations comprising

phase change source terms can be obtained. For simplicity, only the transport equation for the liquid phase is shown.

$$\begin{aligned} & \frac{\partial \alpha_i}{\partial t} + \nabla \cdot (\alpha_i U) + \nabla \cdot (\alpha_i \alpha_v (U_i - U_v) + \alpha_i \alpha_i (U_i - U_i)) \\ &= -\frac{\alpha_i}{\rho_i} \left[\frac{D \rho_i}{D t} \right] (1 - \alpha_i) + \alpha_i (\nabla \cdot U) + \alpha_i \left[\frac{\alpha_v}{\rho_v} \frac{D \rho_v}{D t} + \frac{\alpha_i}{\rho_i} \frac{D \rho_i}{D t} \right] \\ &+ \dot{m} \left(\frac{1}{\rho_i} - \alpha_i \left(\frac{1}{\rho_i} - \frac{1}{\rho_v} \right) \right) \end{aligned} \quad (6)$$

The present study employs VOF with LES turbulence modelling. The VOF-LES is based on a mathematical model composed of governing equations for the conservation of mass and momentum of a multiphase system, accredited to De Villiers *et al.* [2]. This system comprises three immiscible, compressible fluids and accounts for the surface tension between. The details about the VOF-LES formulation can be found in our previous work [4].

Schnerr and Sauer Model

The Schnerr and Sauer model is based on bubble dynamics derived from the generalised Rayleigh-Plesset equation. In the present study, a phase change limiter $m \max(1 - \alpha_i - \alpha_i, 0)$ is added to eliminate unbounded volume fractions caused by physically unrealistic condensation and vaporisation rates. The modified Schnerr and Sauer model is defined as

$$\begin{cases} \dot{m}^- = \frac{3\rho_l \rho_v}{\rho} \alpha_i m \max(1 - \alpha_i - \alpha_i, 0) (rR_b) \\ * \sqrt{\frac{2}{3\rho_l (|p - p_v| + 0.001 p_v)}} m \ln(p - p_v, 0) \\ \dot{m}^+ = \frac{3\rho_l \rho_v}{\rho} \alpha_i m \max(1 - \alpha_i - \alpha_i, 0) (rR_b) \\ * \sqrt{\frac{2}{3\rho_l (|p - p_v| + 0.001 p_v)}} m \max(p - p_v, 0) \end{cases} \quad (7)$$

The reverse of the cavitation nuclei radius rR_b is related to α_i , α_i and bubble density n by

$$rR_b = \left(\frac{4\pi n \alpha_i}{3(m \max(1 - \alpha_i - \alpha_i, 0) + a_{\text{phanuc}})} \right)^{1/3} \quad (8)$$

where the nucleation site volume fraction

$$a_{\text{phanuc}} = \frac{n\pi (d_{\text{Nuc}})^3}{6 + n\pi (d_{\text{Nuc}})^3} \quad (9)$$

is used to avoid division by zero. In the present study, bubble diameter d_{Nuc} is set as $0.1 \mu\text{m}$ (20% of the smallest mesh size $0.47 \mu\text{m}$) and bubble density n is set to $2.0 \times 10^9 \text{ cm}^{-3}$ based on the suggestion of Schnerr *et al.* [8].

Validation of the Numerical Model

The experimental data from Winklhofer *et al.* [13] is used for a comprehensive model validation. In the work of Winklhofer *et al.*, measurements are taken for diesel fuel passing through a $300 \mu\text{m}$ thick square channel where the injection pressure is fixed at 100 bar and the back pressure is varied to change the extent of cavitation from inception through to choked flow. The channel has an inlet width of $301 \mu\text{m}$ and is slightly converging through a length of $1000 \mu\text{m}$ to give an outlet width of $284 \mu\text{m}$. Detailed

geometry for the square channel used in the present study can be found in [13]. Fuel inlet is set at the left end of the geometry, while a simplified non-reflective pressure outlet is applied to the right end. The remaining face patches of the computational domain are configured to be no-slip and adiabatic walls with a zero-gradient boundary condition for all hydrodynamic variables. The cavitation is normally characterised by a global cavitation number (CN) commonly defined as

$$CN = \frac{p_{inj} - p_{out}}{p_{out} - p_v} \quad (10)$$

Detailed properties of the fuel and operating conditions are given in Table 1.

Parameter	Value
Injection pressure	100 bar
Fuel	n-dodecane
Fuel density	832 kg/m ³
Fuel dynamic viscosity	0.0065 N s/m ²
Surface tension	0.03 N/m
Vapour density	0.1361 kg/m ³
Vapour pressure	2000 Pa
Vapour dynamic viscosity	5.953×10^{-6} N s/m ²
Temperature	304 K
Ambient pressure	30-80 bar
Cavitation number	0.25-2.33
Max velocity	150 m/s
Fuel Reynolds number	1817-5452

Table 1: Fuel properties and boundary conditions based on experimental setup [13].

Kolmogorov scale representing the smallest turbulence scale of the flow can then be estimated using the following formulation

$$\eta = \frac{\bar{W}}{(\text{Re})^{1/4}} \quad (11)$$

where \bar{W} is the channel outlet length and μ the dynamic viscosity of the liquid phase and Re is the liquid phase Reynolds number. However, a single Kolmogorov scale cannot be determined due to density variation in a compressible flow. Thus, only liquid phase's Kolmogorov scale is evaluated to be $0.47 \mu\text{m}$ because liquid fuel is relatively incompressible compared to air and vapour. The mesh is constructed by layering elements from the nozzle wall with a minimum size of $0.5 \mu\text{m}$ and a growth rate of 1.05 as shown in Figure 1. Totally 6 million hexahedral elements are used.

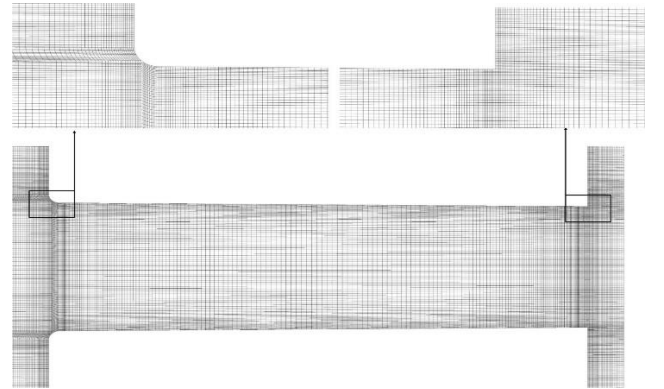


Figure 1: Computational domain for the square channel.

Comparison of simulated and measured mass flow rates at different flow conditions are presented in Figure 2. The developed numerical model captures the effect of pressure on mass flow rates with favourable accuracy. The trend that mass

flow rate increases almost linearly with increasing difference between injection and back pressures is also well captured. When the difference between injection and back pressures has exceeded 70 bar ($\Delta p > 70 \text{ bar}$), both experiment and simulation show that further reducing the back pressure has only a minor effect on the rate of injection. This is because, at $\Delta p = 70 \text{ bar}$, the flow has become choked (e.g. mass flow rate does not increase with decrease in back pressure).

As shown in Figure 3, reduction in pressure downstream of the channel entrance before cavitation inception is demonstrated by both simulation and experiment. The extent of low pressure region simulated is consistent with experimental measurements. Cavitation inception occurs when the back pressure is set to 40 bar (Figure 3(b)). As the back pressure decreases, vapour cavities start to form in the recirculation zone and build up along the channel wall. At 30 bar back pressure the flow is fully choked and complete separation of flow from the channel entrance occurs (Figure 3(c)). Deviation between simulations and experiments, in terms of extent and morphology of the cavitation, can be attributed to uncertainties in fluid properties, omission of surface imperfections on the round entrance and channel wall in the numerical model. These uncertainties, however, are difficult to eliminate in numerical simulations due to limited computing power.

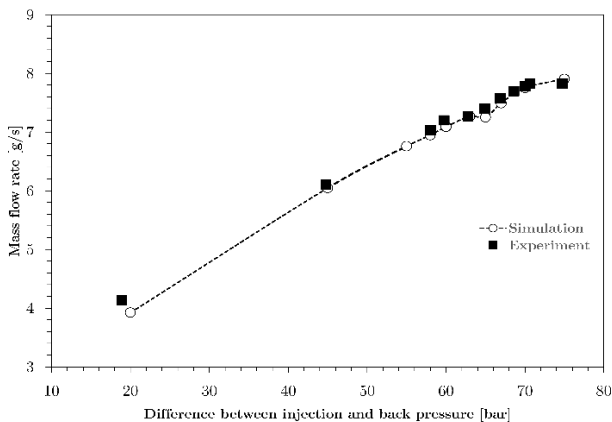


Figure 2: Comparison of simulated and measured mass flow rates at different back pressure conditions

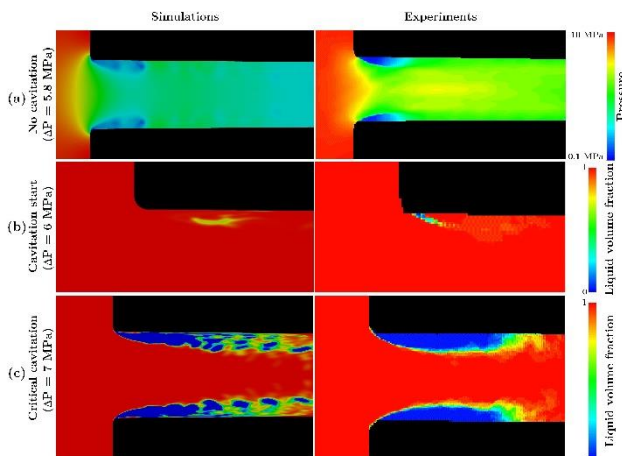


Figure 3: Comparison of averaged contour plots of simulated (time averaged) and measured (averaged over 20 images) pressure and liquid volume fraction distribution in the channel at $\Delta p = 58, 60$ and 70 bar.

Characterisation of nozzle flow and primary breakup

Experimental conditions summarised in Ghiji *et al.*[4], relevant for a non-evaporating spray injected into a constant volume

chamber from a sharp edged nozzle are simulated. The properties of the diesel fuel and vapour, except for the temperature and Reynolds number, are given in Table 1. The ambient region (chamber) is non-reactive and initially filled with compressed air at 30 bar. The computational domain representing a diesel injector includes the sac, nozzle and a portion of the chamber is shown in Figure 4. Boundary conditions are similar to the experimental setup of Ghiji *et al.* [4]. However, due to the lack of detailed knowledge of the time varying pressure profile in the injector sac, the pressure at the sac inlet is assumed to increase linearly from 30bar to 600bar in $100 \mu s$.

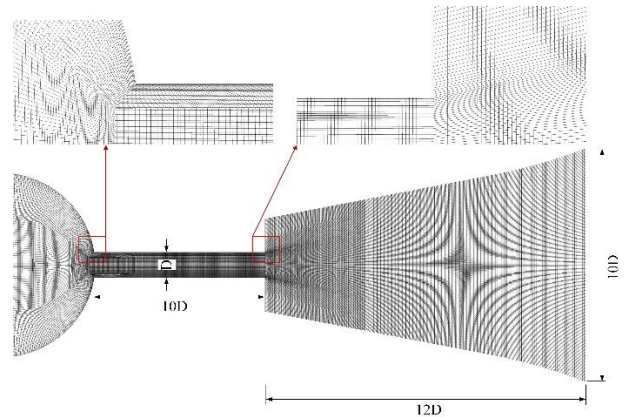


Figure 4: Dimensions and mesh topology for the computational domain. Refined hexahedral elements of $0.7 \mu m$ (based on Kolmogorov scale for the developed spray) are distributed in the nozzle at the wall. The mesh size increases gradually from the nozzle with a grow rate of 1.02. In total, 12 million hexahedral elements.

The penetrating spray and the nozzle flow are represented in Figure 5 by a liquid volume fraction isosurface ($\alpha = 0.9$) coloured by velocity magnitude. At $19 \mu s$ After Start of Injection (ASOI), the emerging spray predicted by the two models is of similar shape. The mushroom like structure at the leading edge is the result of interaction of the compressed air ahead of the penetrating tip and the liquid jet. Surface instabilities start to develop at the edge of the mushroom structure and only minor disturbances are observed on the liquid surface. At $20 \mu s$ ASOI, a ring of cavitation bubbles is predicted by the cavitation model in the separation region near the nozzle entrance. By $37 \mu s$ ASOI aerodynamic forces start to strip small scale structures such as liquid ligaments and droplets from the liquid surface in the wake and at the edge of the 'mushroom'. In-nozzle turbulence and cavities have grown in the boundary layer and cavitation bubbles are emerging from the nozzle. The collapse of the cavitation bubble generated from an early stage and the in-nozzle turbulence enhance surface instabilities on the jet. The non-cavitating code predicts a much less disturbed exiting jet. However, the opposite trend is observed after the occurrence of complete flow detachment when wall shear disappears in the cavitation simulation at $56 \mu s$ ASOI. After this transition to hydraulic flip, the cavitation model predicts that the spray dispersion is narrowed and there is an intact liquid core leaving the nozzle exit. The near wall region is completely filled with mixtures composed of liquid, vapour and ambient gas connected to the chamber. At this stage the non-cavitating code captures a more turbulent exiting jet than the cavitation models. This is attributed to the persistent presence of wall shear which introduces turbulent disturbances on the surface of the jet

Details in the vapour collapse region of the jet are resolved in Figure 6 which shows sectional contour plots of diesel volume fraction, total pressure and rate of condensation at $37 \mu s$ ASOI. Once cavities extend outside the nozzle exit, they collapse within

the liquid jet with pressure recovery. However, low pressure regions appear where cavities collapse. This may be attributable to liquid inertia and cavity oscillations. Localised low pressure regions and convex surface protrusions are observed to correlate spatially with regions of high vapour condensation rate. The presence and collapse of cavities within the liquid jet creates pressure gradients, as observed by Schnerr *et al.*[9]. The presence of collapsing cavitation bubbles within the emerging jet suggests they play a role in the greater development of surface instabilities and breakup in the cavitating cases compared with the non-cavitating despite the presence of turbulence.

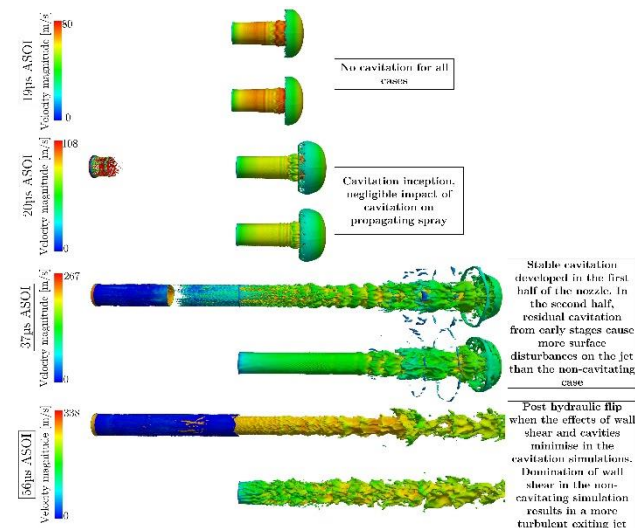


Figure 5: Penetrating spray represented by a liquid volume isosurface ($\alpha = 0.9$) coloured by velocity magnitude. Top: Schnerr, Bottom: Non-cavitating.

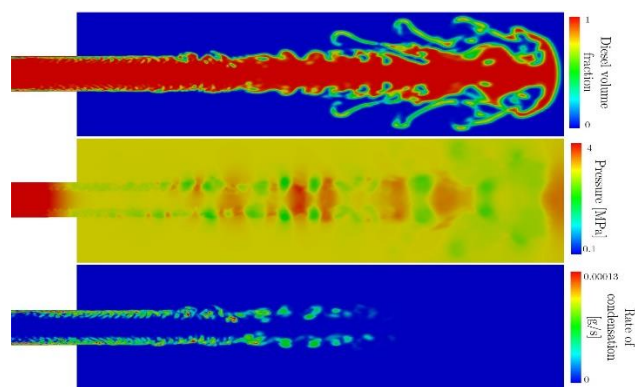


Figure 6: Sectional contour plots of diesel volume fraction, total pressure and rate of condensation at $37 \mu\text{s}$ ASOI. Localised low pressure regions and convex surface protrusions are observed to correlate spatially with regions of high vapour condensation rate.

Conclusions

The onset of in-nozzle cavitation and its effects on the morphology of early spray is successfully characterised using a compressible multiphase VOF cavitation LES code. The numerical simulations reveal that:

- The pressure in the contraction region can reduce to vapour pressure, leading to vaporisation of fuel and formation of vapour cavities.
- Vapour cavities forming at the nozzle inlet can grow to an extent that detaching bubbles collapse within the liquid jet after exiting the nozzle, enhancing jet breakup.

- By comparing cavitating and non-cavitating simulations, it is apparent that apart from in-nozzle flow separation and cavitation, another important factor contributing to the primary breakup of the spray is the wall shear experienced by the jet in the nozzle.

Acknowledgments

Significant support was received from the Australian Maritime College in terms of the access to the high performance computer clusters and installation of Open-Foam. The authors express their gratitude to Zhi Quan Leong for his support and suggestions.

References

- [1] Andriotis, A., & Gavaises, M. (2009). Influence of vortex flow and cavitation on near-nozzle diesel spray dispersion angle. *Atomization and Sprays*, 19(3).
- [2] De Villiers, E., Gosman, A., & Weller, H. (2004). Large eddy simulation of primary diesel spray atomization. *SAE transactions*, 113(3), 193-206.
- [3] Gavaises, M., & Andriotis, A. (2006). Cavitation inside multi-hole injectors for large diesel engines and its effect on the near-nozzle spray structure: SAE Technical Paper.
- [4] Ghiji, M., Goldsworthy, L., Brandner, P., Garaniya, V., & Hield, P. (2016). Numerical and experimental investigation of early stage diesel sprays. *Fuel*, 175, 274-286.
- [5] Giannadakis, E., Gavaises, M., Roth, H., & Arcoumanis, C. (2004). *Cavitation modelling in single-hole Diesel injector based on eulerian-lagrangian approach*. Paper presented at the Proc. THIESEL International Conference on Thermo- and Fluid Dynamic Processes in Diesel Engines. Valencia, Spain.
- [6] Grogger, H., & Alajbegovic, A. (1998). Calculation of the cavitating flow in venturi geometries using two fluid model. *ASME Paper FEDSM*, 5295.
- [7] Marcer, R., Le Cottier, P., Chaves, H., Argueyrolles, B., Habchi, C., & Barbeau, B. (2000). A validated numerical simulation of diesel injector flow using a VOF method: SAE Technical Paper.
- [8] Schnerr, G. H., & Sauer, J. (2001). *Physical and numerical modeling of unsteady cavitation dynamics*. Paper presented at the Fourth international conference on multiphase flow, New Orleans, USA.
- [9] Schnerr, G. H., Schmidt, S. J., Sezal, I. H., & Thalhamer, M. (2006). *Shock and wave dynamics of compressible liquid flows with special emphasis on unsteady load on hydrofoils and on cavitation in injection nozzles*. Paper presented at the Proceedings of 6th International Symposium on Cavitation, Wageningen, The Netherlands.
- [10] Som, S., Aggarwal, S., El-Hannouny, E., & Longman, D. (2010). Investigation of nozzle flow and cavitation characteristics in a diesel injector. *Journal of Engineering for Gas Turbines and Power*, 132(4), 042802.
- [11] Tamaki, N., Nishida, K., Hiroyasu, H., & Shimizu, M. (1997). Effects of the internal flow in a nozzle hole on the breakup processes of a liquid jet. *International Journal of Fluid Mechanics Research*, 24(4-6).
- [12] Westlye, F. R., Battistoni, M., Skeen, S., Manin, J., Pickett, L. M., & Ivarsson, A. (2016). Penetration and Combustion Characterization of Cavitating and Non-Cavitating Fuel Injectors: SAE Technical Paper.
- [13] Winklhofer, E., Kull, E., Kelz, E., & Morozov, A. (2001). *Comprehensive hydraulic and flow field documentation in model throttle experiments under cavitation conditions*. Paper presented at the Proceedings of the ILASS-Europe conference, Zurich.